Label-Free Raman Spectromicroscopy Unravels the Relationship between MGMT Methylation and Intracellular Lipid Accumulation in Glioblastoma

Nana Wang[a][§], Jiejun Wang[b][§], Pu Wang[a], Nan Ji[b][*], and Shuhua Yue[a][*]

[a]*Key Laboratory of Biomechanics and Mechanobiology (Beihang University), Ministry of Education, Institute of Medical Photonics, Beijing Advanced Innovation Center for Biomedical Engineering, School of Biological Science and Medical Engineering, Beihang University, Beijing, 100191, China.*

[b]*Department of Neurosurgery, Beijing Tiantan Hospital, Capital Medical University, Beijing, 100070, China.*

*Email: yue_shuhua@buaa.edu.cn (S.Y.); jinan@mail.ccmu.edu.cn (N.J.).

§ Equally contributed to this work.

Table of Content

Materials and Methods

Human Glioblastoma (GBM) Tissue Specimens

This study was approved by institutional review board. All samples derived from 36 patients diagnosed with GBM multiforme in Neurosurgery Department of Beijing Tiantan Hospital. All specimens of cancerous tissues were collected from patients during resection surgery and directly stored in liquid nitrogen. Subsequently, for each tissue specimen, pairs of neighboring slices were prepared, with one slice remained unstained for spectroscopic imaging and the other stained with hematoxylin and eosin (H&E). Pathological examination was made by neurosurgical pathologists.

Preparation of Lipid Droplet (LD) Emulsions

Considering that the neutral lipids in LDs are primarily composed of triglycerides (TGs) and cholesteryl esters (CEs), we made LD emulsions with known molar ratios of TG and CE as described previously.[1, 2] Glyceryl trioleate (Sigma-Aldrich) was used as the TG representative and cholesteryl oleate (Sigma-Aldrich) was used as the CE representative. Briefly, cholesteryl oleate and glyceryl trioleate were separately dissolved in acetone at the same concentration (10 mM). The cholesteryl oleate and glyceryl trioleate solutions were mixed together at various volume ratios, including eleven different CE:TG molar ratios, ranging from 0:10 to 10:0. The mixtures were then added into deionized water at a volume ratio of 1:20, supplemented with 0.05% Tween-20 surfactant. LDs formed after magnetic stirring for 10 min. A drop of emulsion solution (~2 μL) was sandwiched between two glass coverslips and sealed right before imaging and spectral analysis.

Label-free Raman Spectromicroscopy

In our multimodal NLO microscopy setup, we employed a picosecond pulse laser (picoEmerald™S, Applied Physics &Electronics) with 80 MHz repetition rate and 2 picosecond pulse width, as described previously.[3] The laser has an integrated output for both the pump beam with tunable wavelength from 700 nm to 960 nm and the Stokes beam with fixed wavelength at 1031 nm, which are overlapped in space and time. When performing SRS, the Stokes beam was modulated at ~20 MHz by an electronicoptic modulator. The collinear pump and Strokes beams were coupled to a two-dimensional scanning galvanometer (GVS012-2D, Thorlab) and then imported into an inverted microscope (IX73, Olympus). The water immersion objective lens (LUMPlanFL N, Olympus) used to focus the light on the sample had a magnification of 60X and a numerical aperture of 1.0. Transmission of the forward-detected SRS signal was acquired by another 60 X water-immersion objective (LUMPlanFL N, 1.0 numerical aperture Olympus). A short-pass filter (ET980SP, Chroma) was used before a 10 mm x 10 mm large area silicon photodiode (S3994-01, Hamamatsu) detector with 48 DC reversed bias voltage. The signal was then extracted by a lock-in amplifier (HF2LI, Zurich Instruments). The analog output representing the SRS signal was fed into a data acquisition card (PCIE-6363, National Instruments) and input to the computer to display the image on the LabVIEW 2018 software.

In order to detect the vibrational bands of CH_2 (2850 cm^{-1}) the wavelength of the pump beam was tuned to 796.8 nm. The excitation power at the sample was ~50 mW for pump and ~300 mW for Stokes for all GBM tissues (~20 μm). The SRS images for LDs analysis containing 512 x 512 pixels were collected with a pixel dwell time of 8 μs. The large-scale SRS images were performed by a microscope motorized platform (H117, Prior). No photodamage to tissue was detected. Spontaneous Raman spectra were acquired with a

Raman micro-spectrometer (DR316B-LDC-DD, Andor), which was mounted to the side of the microscope. The pump beam was tuned to ~707 nm for Raman spectra measurements. The excitation power at the sample was ~50 mW and ~60mW for LD emulsions and GBM tissues (~20 μm). Each Raman spectrum ranged from 380 to 3100 cm^{-1} in 30 seconds for LD emulsions and 60 seconds for GBM tissues.

Quantitative Analysis of the Amount and Composition of LDs

We quantitatively analyzed neutral lipids in three aspects, including LD amount, CE percentage and lipid saturation degree. By using ImageJ "Threshold" function, LDs can be extracted based on the significantly higher signal intensities compared to other cellular compartments. Then, by using ImageJ "Analyze Particles" function, fraction of LDs area out of tissue area can be quantified. For tissue specimen, fractions of LDs area from the 8-10 locations were averaged to obtain the final value of LD area fraction. The percentage of CE in individual LDs was linearly correlated with the height ratio of the 702 cm^{-1} peak to the 1442 cm^{-1} peak (I_{702}/I_{1442}). Specifically, I_{702}/I_{1442} = 0.00273 × CE percentage (%). The corresponding calibration curve is shown in Figure S2. For statistical analysis, CE percentage for each specimen was obtained by averaging the CE percentage of LDs in 10~15 areas. Meanwhile, lipid saturation degree in individual LDs was characterized by the height ratio of the 2883 cm^{-1} peak to the 2850 cm^{-1} peak (I_{2883}/I_{2850}). For statistical analysis, the height ratio (I_{2883}/I_{2850}) for each specimen was obtained by averaging the height ratio (I_{2883}/I_{2850}) of LDs in 10~15 areas.

Public Dataset

The Cancer Genome Atlas (TCGA), a project supported by the National Cancer Institute (NCI) and National Human Genome Research Institute (NHGRI), has generated comprehensive, multi-dimensional maps of the key genomic changes in various types of cancers. The GBM dataset in TCGA-GBM, including DNA methylation, gene expression and survival data, was obtained from the UCSC Xena browser (https://xenabrowser.net).[4] We obtained 77 GBM cases, who contained survival, DNA methylation and Gene expression data.

Differentially Expressed Genes (DEGs) Analysis

The principle of differential analysis is to first convert the count matrix into an object, then each gene gets assigned the same dispersion estimate, then performs pair-wise tests for differential expression between two groups, and finally takes the output using the False Discovery Rate (FDR) correction, and returns the top differentially expressed genes. The parameters set for differential expression analysis were FDR < 0.05 with |Log$_2$FC| > 2. Subsequently, Gene Ontology (GO) analysis was used to do the biological function analysis. R programming language was used to analyze the correlation between O^6-methylguanine-DNA methyltransferase (MGMT) expression and other genes expression with the Pearson correlation analysis. The figures were plotted with the GraphPad prism9.

Statistical Analysis

All data were shown as mean ± standard error of the mean (SEM). One-way ANOVA was used for comparisons of LD area fraction, CE percentage and height ratio (I_{2883}/I_{2850}) among different groups. P value

< 0.05 was considered statistically significant. Comparisons of overall survival (%) among groups were performed with the log-rank test.
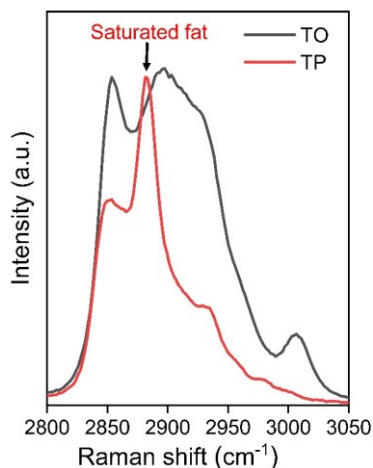
Supporting Figures

Figure S1. The Raman spectra of glyceryl tripalmitate (TP) and glyceryl trioleate (TO) in CH vibrational region. The characteristic Raman peak at 2883 cm^{-1} indicates the presence of saturated fats.
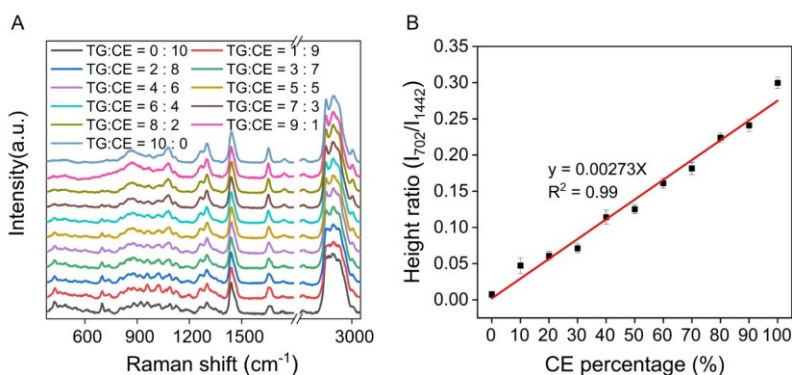

Figure S2. The calibration curve of CE/TG emulsions. (A) Raman spectra of CE/TG emulsions with eleven different CE:TG molar ratios, ranging from 0:10 to 10:0. CE/TG emulsions are mixtures of cholesteryl oleate and glyceryl trioleate and used as the standards of certain CE molar percentage. Spectral intensity was normalized by the peak at 1442 cm^{-1}. (B) Calibration curve for quantification of molar percentage of CE out of total neutral lipid, generated by linear fitting of height ratio between the peak at 702 cm^{-1} and the peak at 1442 cm^{-1}. Height ratio = 0.00273 × CE percentage (%). The intercept was set to 0 for linear fitting.
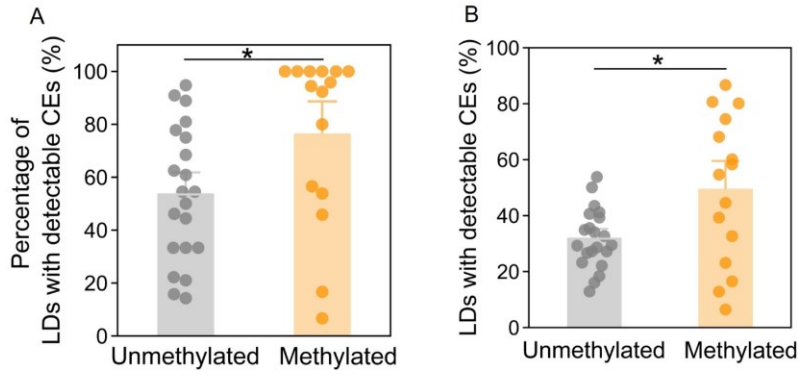
Figure S3. The relationship between quantification of LDs and MGMT methylation. (A) Percentage of intracellular LDs with detectable CEs derived in GBM tissues from 36 patients. (B) The fraction of LDs with detectable CEs in unmethylated or methylated GBM tissues. Each dot in (A) represents average percentage of LDs with detectable CEs for one patient. Each dot in (B) represents average the fraction of LDs with detectable CEs for one patient. Error bars represent SEM, n>10. One-way ANOVA, *p < 0.05.
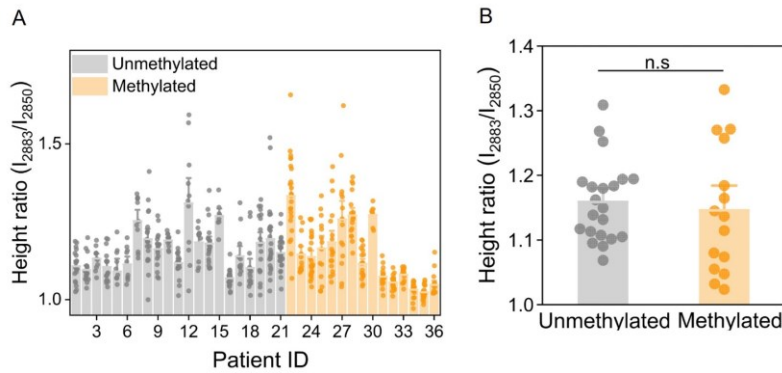
Figure S4. Quantitative analysis of the correlation between MGMT methylation and lipid accumulation in GBM. (A) The level of height ratio (I_{2883}/I_{2850}) was analyzed in GBM tissues from 36 patients. (B) Average quantification of height ratio (I_{2883}/I_{2850}) in (A) for unmethylated or methylated group. Each dot in (B) represents the average height ratio (I_{2883}/I_{2850}) for one patient. Error bars represent SEM, n > 10.
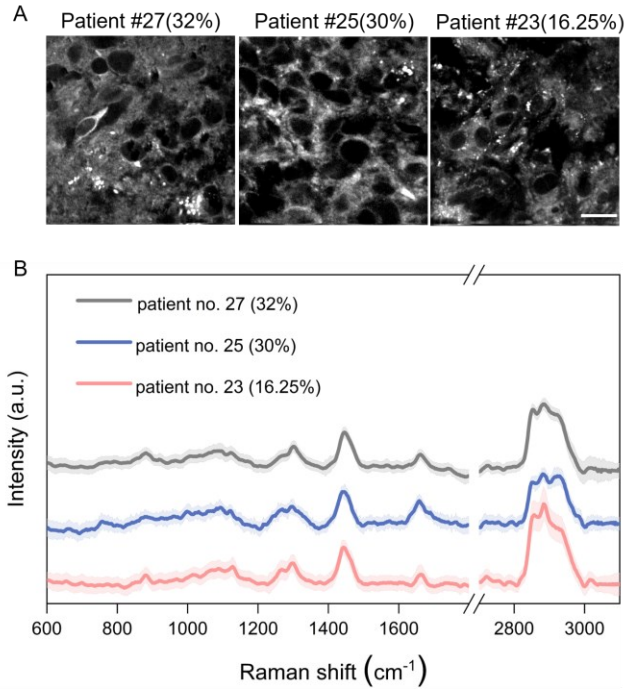
Figure S5. LDs showed no significant regularity in methylated GBMs. (A) Representative SRS images of methylated GBM tissues, appearing low in some patients. Scale bar: 20 μm. (B) Representative Raman spectra of LDs in GBM shown in (A). Spectral intensity was normalized by CH_2 bending band at 1442 cm^{-1}. Shaded area indicates the standard deviation of Raman spectral measurements from different LDs in the same GBM tissue.

MGMT methylation	Number at risk				
≥50%	5	5	3	1	0	0
≥40%	12	11	5	2	2	0
≥30%	21	15	8	3	2	0
≥15%	31	22	12	5	2	0
<15%	46	25	4	2	0	0

MGMT methylation	≥50%	≥40%	≥30%	≥15%	<15%
Madian survival (months)	21.1	16.6	16.1	16.6	12.5

Figure S6. The relationship between OS and MGMT methylation base on TCGA dataset. (A) Kaplan–Meier estimates of OS among patients with GBM from TCGA dataset. (B) The relationship between OS and MGMT methylation was also evaluated with Kaplan-Meier method. Log-rank test p < 0.005.

Figure S7. The fraction of LDs with detectable CEs in the hypermethylated, intermediate-methylated and unmethylated groups. Each dot represents average the fraction of LDs with detectable CEs for one patient. Error bars represent SEM, n > 10. One-way ANOVA, *p < 0.05, **p < 0.005, ***p < 0.0005.
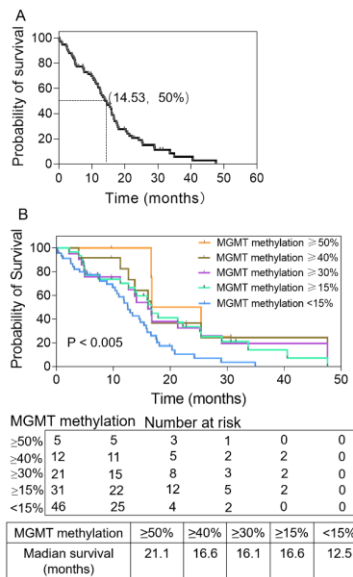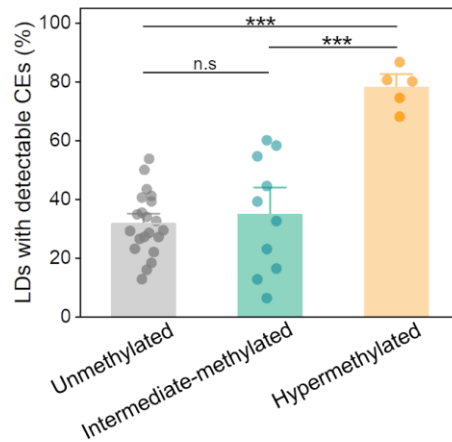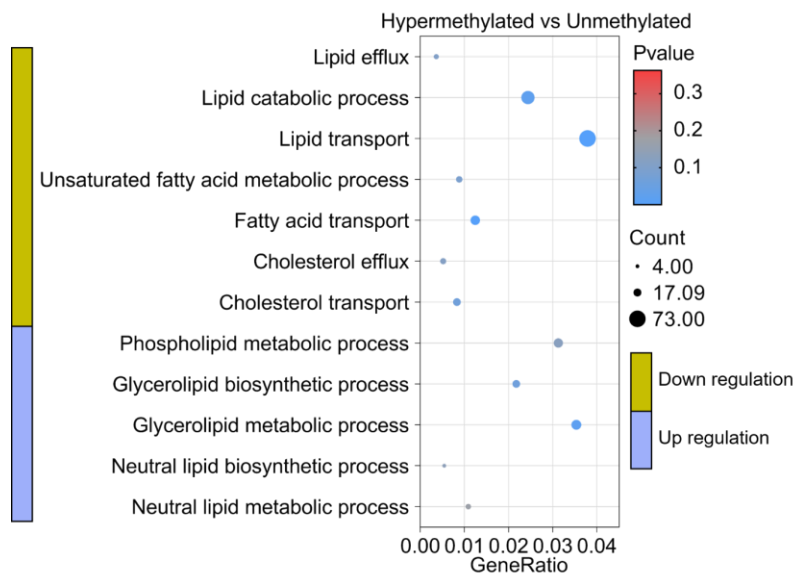

Figure S8. GO enrichment analysis of DEGs associating with lipid metabolism in Hypermethylated vs Unmethylated group.
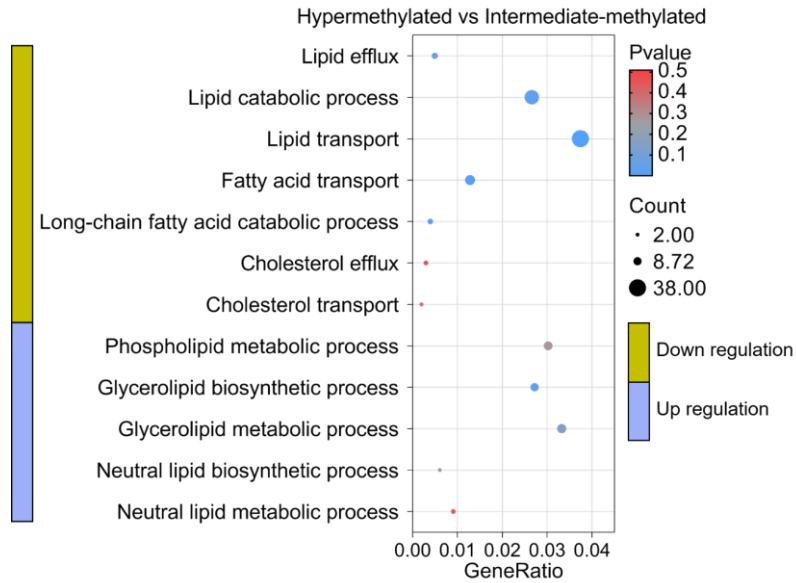
Figure S9. GO enrichment analysis of DEGs associating with lipid metabolism in Hypermethylated vs Intermediate-methylated group.
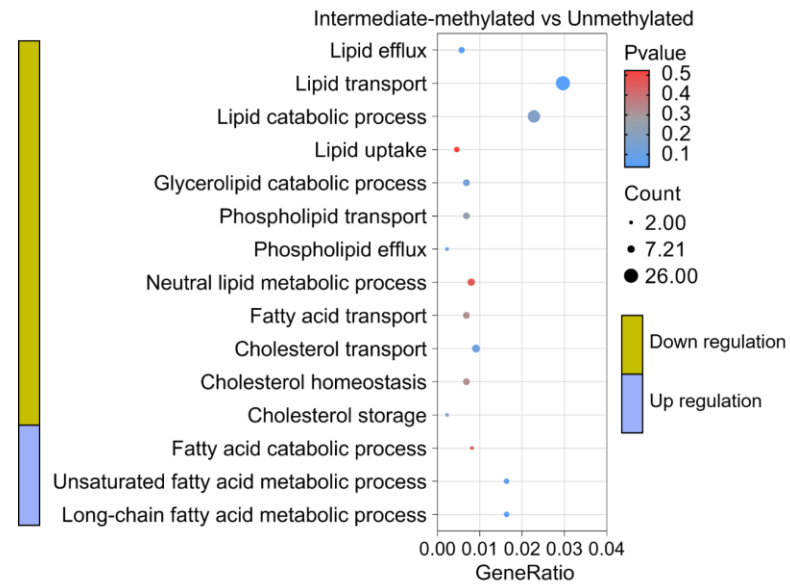

Figure S10. GO enrichment analysis of DEGs associating with lipid metabolism in Hypermethylated vs Intermediate-methylated group.

Table S1. LD area fraction, molar percentage of CE in LDs and the level of height ratio (I_{2883}/I_{2850}) from 36 GBM patients

Patient ID	MGMT methylation	LD area fraction (%)	LD area fraction Mean ± SEM (%)	CE percentage (%)	CE percentage Mean ± SEM (%)	I_{2883}/I_{2850}	I_{2883}/I_{2850} Mean ± SEM (%)
1	2.75%	1.49		38.92		1.11	
2	3.00%	1.60		26.51		1.10	
3	3.00%	1.18		19.39		1.13	
4	3.25%	1.33		16.11		1.10	
5	3.25%	0.76		9.09		1.09	
6	3.25%	0.53		4.91		1.11	
7	3.50%	2.95		21.44		1.25	
8	3.50%	1.40		15.51		1.19	
9	4.00%	1.25		7.01		1.16	
10	4.00%	1.53		25.43		1.19	
11	4.75%	1.64	1.37 ± 0.15	32.91	18.17 ± 2.51	1.12	1.16 ± 0.01
12	4.75%	0.78		5.35		1.31	
13	4.75%	1.15		17.93		1.18	
14	5.00%	2.37		18.62		1.18	
15	5.25%	1.03		6.19		1.27	
16	6.00%	3.04		45.53		1.07	
17	6.00%	0.76		7.74		1.14	
18	6.75%	0.67		22.14		1.10	
19	7.50%	1.09		2.91		1.18	
20	10.25%	0.71		24.48		1.19	
21	12.00%	1.45		13.51		1.15	
22	15.50%	0.92		7.57		1.33	
23	16.25%	1.16		17.58		1.14	
24	17.25%	2.32		44.54		1.14	
25	30.00%	0.31		15.27		1.16	
26	30.00%	2.96	1.62 ± 0.33	55.07	25.10 ± 7.15	1.18	1.19 ± 0.03
27	32.00%	0.95		0.86		1.25	
28	32.25%	1.70		3.85		1.27	
29	45.75%	2.57		50.46		1.11	
30	46.50%	0.34		3.67		1.27	
31	47.75%	3.01		52.10		1.07	
32	54.50%	7.47		74.50		1.06	
33	61.75%	7.65		68.15		1.08	
34	65.75%	7.88	7.79 ± 0.24	86.68	78.01 ± 3.13	1.03	1.05 ± 0.01
35	71.00%	8.65		80.61		1.02	
36	78.50%	7.28		80.11		1.05	

SEM = standard error of the mean

References

1. Wang, P.; Li, J.; Wang, P.; Hu, C, R.; Zhang, D.; Sturek, M.; Cheng, J, X. Label-Free Quantitative Imaging of Cholesterol in Intact Tissues by Hyperspectral Stimulated Raman Scattering Microscopy. *Angew. Chem. Int. Ed. Engl.* 2013, 52(49), 13042-13046.

2. Yue, S.; Li, J.; Lee, S. Y.; Lee, H. J.; Shao, T.; Song, B.; Cheng, L.; Masterson, T. A.; Liu, X.; Ratliff, T. L.; Cheng, J. X. Cholesteryl Ester Accumulation Induced by PTEN Loss and PI3K/AKT Activation Underlies Human Prostate Cancer Aggressiveness. *Cell. Metab.* 2014, 19 (3), 393-406.

3. Jia, H.; Liu, J.; Fang, T; Zhou, Z.; Li, R.; Yin, W.; Qian, Y.; Wang, Q.; Zhou, W.; Liu, C.; Sun, D.; Chen, X.; Ou, Y, Z.; Dong, J.; Wang, Y.; Yue, S. The Role of Altered Lipid Composition and Distribution in Liver Fibrosis Revealed by Multimodal Nonlinear Optical Microscopy. *Sci Adv.* 2023, 9(2), eabq2937.

4. Goldman, M. J.; Craft, B.; Hastie, M.; Repečka, K.; McDade, F.; Kamath, A.; Banerjee, A.; Luo, Y.; Rogers, D.; Brooks, A. N.; Zhu, J.; Haussler, D. Visualizing and Interpreting Cancer Genomics Data via the Xena Platform. *Nat. Biotechnol.* 2020, 38(6), 675-678.